Editors' Suggestion

Asymmetric rectified electric fields generate flows that can dominate induced-charge electrokinetics

S. M. H. Hashemi Amrei, Gregory H. Miller,* and William D. Ristenpart†
Department of Chemical Engineering, University of California Davis, Davis, California 95616, United States

(Received 16 July 2019; published 8 January 2020)

We derive a generalized induced-charge electrokinetic (ICEK) velocity around a conducting object placed in an arbitrary multimodal electric field. The generalized model allows consideration of asymmetric rectified electric fields (AREFs), which have recently been established to occur in liquids where the ions present have unequal mobilities. Including the AREF yields fluid velocities in which both the direction and the magnitude depend sensitively on the applied potential, frequency, ionic type and strength, and even the exact placement of the object between parallel electrodes. The results provide an explanation for the long-standing question of flow reversals observed in ICEK systems.

DOI: 10.1103/PhysRevFluids.5.013702

I. INTRODUCTION

Nonlinear electroosmotic flows around colloidal particles, also known as electrokinetic phenomena of the second kind, were first formulated theoretically by Dukhin and co-workers in the 1980s [1–3]. They demonstrated that application of an external electric field induces a charge cloud near the surface of a polarizable object; the field then creates a body force on the charge cloud, creating an electroosmotic fluid flow. In contrast to standard electroosmosis, the fluid velocity scales as the square of the electric field, so that flow results from both steady and oscillatory applied fields. One early application of nonlinear electroosmotic flows was liquid pumping via asymmetric electrodes subject to AC electric potentials, also known as AC electroosmosis (ACEO) [4–7]. More recently, Bazant and Squires [8,9] unified nonlinear electrokinetic phenomena around polarizable objects (particles, electrodes, etc.) under the name induced-charge electrokinetics (ICEK) [10–13]. The general theoretical approach has been to solve either the Laplace equation or the standard electrokinetic model (Poisson-Nernst-Planck) to predict the electric field distribution and polarization of the charge layer around the objects, and then determine the induced flow. The archetypal example of ICEK theory is the quadrupolar fluid flow around a conducting sphere or cylinder in response to steady or time varying electric fields [8,9], a system which has been experimentally observed in a number of studies using metallic spheres [14,15] and wires [16–18].

Despite extensive research, however, there are several unresolved discrepancies between theoretical predictions and experimental observations [10,11]. In particular, extant theories fail to predict the observed reversal in the direction of fluid flow in ACEO pumps at sufficiently high frequencies [7,19–22]. Similarly, experimental work revealed that the flow direction in ACEO pumps also depends on the identity of the electrolyte present; for example, at particular voltages and frequencies, simply swapping KCl with KOH caused the flow to reverse direction. Because neither the frequency nor electrolyte dependence are explicable in terms of the standard ICEK theory, much work focused on whether the continuum approximation incorrectly neglected ion-ion

*grgmiller@ucdavis.edu
†wdristenpart@ucdavis.edu

interactions and steric effects, thus yielding unrealistically high ion concentrations near the electrodes [21,23–26]. By introducing the effective ion size as a fitting parameter, Bazant and co-workers qualitatively predicted a fluid flow reversal in AC electroosmosis pumps upon changing the applied frequency. However, an unrealistically large ion size (several nanometers) was found to be necessary, casting doubt on this approach.

Notably, all theoretical studies on ICEK to date have assumed that the dissolved ions have equal mobilities, an assumption that considerably simplifies the modeling but rarely pertains to real electrolytes. Recent work by Hashemi Amrei *et al.* [27,28] has demonstrated that application of a perfectly sinusoidal oscillating potential generates a highly multimodal, long-range electric field between parallel electrodes. Furthermore, if the ions present have unequal mobilities, the multimodal field has a nonzero time average, i.e., the sinusoidal applied potential generates a steady field component. This phenomenon, referred to as an asymmetric rectified electric field (AREF), acts like a dc field and induces electrophoretic motion consistent with experimental observations of particle levitation against gravity [29]. These findings suggest that AREFs will also generate a net fluid flow around a charged object placed in the field via electroosmosis, and thus affect ICEK flows. It remains unclear, however, under what conditions AREFs play a significant role in ICEK flows, and whether they are associated with the flow reversals observed experimentally.

In this work, we analyze theoretically the impact of AREFs on ICEK flows. Because extant theories only consider unimodal electric fields, we begin by deriving a generalized ICEK model valid for arbitrary, multimodal electric fields. We then insert numerical solutions to the fully nonlinear standard electrokinetic model to assess the impact of AREFs on the ICEK flow. Focusing on the flow around a conductive cylinder, we demonstrate that under many conditions the higher order modes and the zeroth mode (the AREF) dominate the overall flow velocity around the cylinder. In particular, the calculations predict significant flow reversals with respect to frequency, electrolyte type, and even the exact placement of the cylinder between conducting electrodes. Our results point toward a resolution of the long-standing discrepancies between ICEK theory and experiments.

II. GENERALIZED ICEK FOR ARBITRARY ELECTRIC FIELD

The central idea of ICEK is that the electric field induces a charge cloud (or an equivalent zeta potential) immediately adjacent to a conductive surface. The tangential component of the same electric field then acts on the induced charge cloud, creating an electroosmotic fluid flow with a slip velocity given by Smoluchowski's formula. Bazant and Squires [8,9] showed that for a steady electric field of magnitude E, i.e., $E(t) = E$, the angular slip velocity around a conductive cylinder of radius a is

$$u_\theta^s = 2\frac{\varepsilon a E^2}{\mu}\sin(2\theta) + 2\frac{\varepsilon \zeta_0 E}{\mu}\sin(\theta), \tag{1}$$

where θ is the polar angle (cf. Fig. 1), ε and μ are the permittivity and viscosity of the electrolyte, respectively, and ζ_0 is the intrinsic zeta potential of the cylinder surface. The first term on the right-hand side is the quadrupolar flow due to the action of the tangential component of the electric field on the surface of the cylinder ($E_\theta|_{r=a}$) on the induced zeta potential, while the second term is the dipolar flow due to the same field acting on the intrinsic zeta potential. Depending on the relative strength of these two terms, various net flows of different shapes that are more or less quadrupolar occur for a steady applied electric field.

In contrast, for a sinusoidal electric field of amplitude E and angular frequency ω_0, i.e., $E(t) = E\cos(\omega_0 t)$, the time average of the slip velocity is [8,9]

$$\left\langle u_\theta^s \right\rangle = \frac{\varepsilon a E^2}{\mu}\frac{\sin(2\theta)}{\omega_0^2\tau_c^2 + 1}. \tag{2}$$

Here $\tau_c = \kappa^{-1}a/\hat{D}$ is the charging time scale of the ionic cloud around the cylinder, where κ^{-1} is the Debye length scale and $\hat{D}$ is a characteristic diffusivity of the dissolved ions. Importantly,

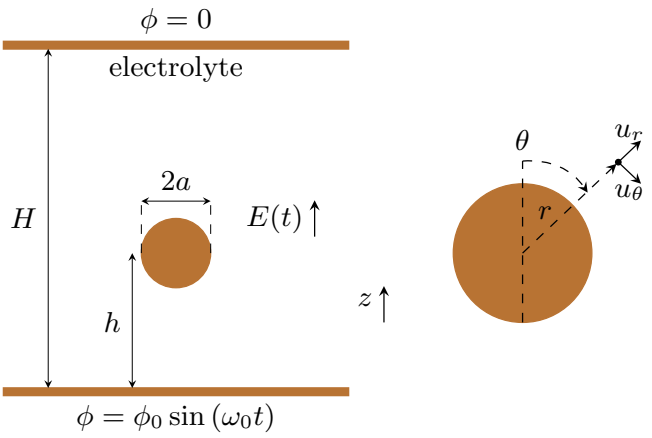

FIG. 1. Schematic diagram of the problem. Left: a conducting cylinder of radius a is immersed in an electrolyte between two parallel electrodes at height h. An oscillatory electric potential is applied on one electrode while the other is grounded. Right: problem in cylindrical coordinates with scalar velocity components in r and θ directions.

the electroosmotic flow due to the action of the sinusoidally varying electric field on the constant intrinsic zeta potential has zero time average, and hence the dipolar component is identically zero for a unimodal applied field. Note also that the velocity is expected to decay monotonically as frequency increases or the electrolyte diffusivity decreases, i.e., no reversals in the flow direction are predicted to occur as frequency changes or for different electrolytes.

We now ask, what happens if the applied field is multimodal? We follow the same basic framework proposed by Bazant and Squires [8,9], but we generalize it to find the slip velocity when $E(t)$ is an arbitrary function of time. Assuming a thin double layer limit ($\kappa a \gg 1$), the solution to the Laplace equation for the electric potential around the cylinder is

$$\psi = -E(t) r \cos(\theta)\left(1 + g\frac{a^2}{r^2}\right), \tag{3}$$

where g is the induced dipole strength, and (r, θ) are the cylindrical coordinates (cf. Fig. 1). The induced surface charge on the cylinder, q, obeys charge conservation such that conduction of ions from the bulk in the radial direction are balanced by charge accumulation, such that

$$\frac{\partial q}{\partial t} = \sigma E_r|_{r=a} = \sigma E(t)\cos(\theta)(1 - g). \tag{4}$$

Here σ is the effective electrolyte conductivity and $E_r = -\frac{\partial \psi}{\partial r}$ is the radial component of the electric field. Simultaneously, the induced zeta potential is

$$\zeta = -\psi|_{r=a} = E(t) a \cos(\theta)(1 + g), \tag{5}$$

where we assumed that electric potential of the perfectly conducting cylinder remains zero at all times. The induced zeta potential is then related to the surface charge with $q = \varepsilon\kappa\zeta$. Note that this equality is justified only at low voltages and is used for simplicity; use of more sophisticated models is straightforward but complicates interpretation. Substituting this equality into Eq. (5) and differentiation with respect to time yields

$$\frac{\partial q}{\partial t} = \varepsilon\kappa a \cos(\theta)\left[\frac{dE(t)}{dt}(1 + g) + E(t)\frac{dg}{dt}\right]. \tag{6}$$

Combining Eqs. (4) and (6) yields an ordinary differential equation for g that can be solved for an arbitrary electric field $E(t)$,

$$g = 2\frac{\int e^{\hat{t}} E(\hat{t})\, d\hat{t}}{e^{\hat{t}} E(\hat{t})} - 1, \tag{7}$$

where $\hat{t} = t/\tau_c$ is a dimensionless time, normalized on the charging time scale $\tau_c = \kappa^{-1} a/\hat{D} = \varepsilon\kappa a/\sigma$ [30,31], and the term $\int e^{\hat{t}} E(\hat{t})\, d\hat{t}$ is an indefinite integral. Substituting the obtained induced dipole g into Eq. (3) yields the potential distribution, which is subsequently used to find the induced zeta potential and tangential component of the electric field ($E_\theta = -\frac{1}{r}\frac{\partial \psi}{\partial \theta}$) on the cylinder surface. Finally, Smoluchowski's formula for electroosmosis gives the induced slip velocity for an arbitrary field,

$$u_\theta^s = -\frac{\varepsilon(\zeta + \zeta_0) E_\theta|_{r=a}}{\mu} = \frac{2\varepsilon a}{\mu}\left[\frac{\int e^{\hat{t}} E(\hat{t})\, d\hat{t}}{e^{\hat{t}}}\right]^2 \sin(2\theta) + \frac{2\varepsilon\zeta_0}{\mu}\left[\frac{\int e^{\hat{t}} E(\hat{t})\, d\hat{t}}{e^{\hat{t}}}\right] \sin(\theta). \tag{8}$$

If the product $e^{\hat{t}} E(\hat{t})$ is simply integrable, then analytical simplifications are straightforward. For a steady (time invariant) applied field, Eq. (1) is immediately recovered. Likewise, for a unimodal oscillating field $E(t) = E\cos(\omega_0 t)$, the instantaneous slip velocity is

$$u_\theta^s = \frac{2\varepsilon a E^2}{\mu}\left[\frac{\omega_0\tau_c \sin(\omega_0 t) + \cos\omega_0 t}{1 + \omega_0^2\tau_c^2}\right]^2 \sin(2\theta) + \frac{2\varepsilon\zeta_0 E}{\mu}\left[\frac{\omega_0\tau_c \sin(\omega_0 t) + \cos\omega_0 t}{1 + \omega_0^2\tau_c^2}\right] \sin(\theta), \tag{9}$$

which upon time averaging reduces to the classic ICEK flow velocity for oscillatory fields [cf. Eq. (2)],

$$\langle u_\theta^s \rangle = \frac{\omega_0}{2\pi}\int_0^{\frac{2\pi}{\omega_0}} u_\theta^s\, dt = \frac{\varepsilon a E^2}{\mu}\frac{\sin(2\theta)}{\omega_0^2\tau_c^2 + 1}. \tag{10}$$

III. SOLUTION TO THE ELECTROKINETIC MODEL

With a generalized ICEK model for arbitrary electric fields in hand, we now ask what happens for the multimodal fields that occur in electrolytes at sufficiently high applied voltages. The details of these fields have been elaborated elsewhere [27,28]; here we provide a brief summary. We focus on 1-1 binary electrolytes between parallel electrodes separated by a distance H (cf. Fig. 1), and we assume that the presence of the cylinder and any resulting flows do not appreciably alter the electric field between parallel electrodes. In other words, we assume that both $a/H \ll 1$ and $a/h \ll 1$ so that we can use the electric field solution $E(t, z)$ in the absence of the cylinder, and we then take $E(t, h)$ (the electric field at the cylinder height, $z = h$) as the field to implement the generalized ICEK velocity. We emphasize that this approach is approximate since it neglects the impact of the cylinder itself on the applied electric field, but our goal is to examine the limiting case of "small" cylinders to shed light on the influence of AREFs on the ICEK flow and to serve as a limiting case for more detailed future calculations.

To obtain the multimodal electric field (in the absence of the cylinder), the Poisson equation relates the free charge density to the electric field gradient,

$$-\varepsilon\frac{\partial^2\phi}{\partial z^2} = e(n_+ - n_-), \tag{11}$$

while the transport of ions is governed by Nernst-Planck equations,

$$\frac{\partial n_\pm}{\partial t} = D_\pm\frac{\partial^2 n_\pm}{\partial z^2} \pm e\frac{D_\pm}{k_B T}\frac{\partial}{\partial z}\left(n_\pm\frac{\partial\phi}{\partial z}\right). \tag{12}$$

Here the symbols stand for permittivity of the electrolyte, ε; electric potential, ϕ; elementary charge, e; number concentration of ion, $n_\pm$; diffusivity, $D_\pm$; Boltzmann constant, k_B; absolute temperature, T; location with respect to the lower electrode, z; and time, t. The terms on the right-hand side of the Nernst-Planck equation represent diffusive (thermal) motion and electromigration of the ions; the nonlinearity of the problem stems from the latter term. To close the problem we apply the initial conditions

$$n_\pm(0,z) = n_\pm^\infty, \tag{13a}$$

$$\phi(0,z) = 0, \tag{13b}$$

and specified potential and no-flux boundary conditions,

$$-D_\pm\left(\frac{\partial n_\pm}{\partial z} \pm \frac{e n_\pm}{k_B T}\frac{\partial \phi}{\partial z}\right)_{z=0,H} = 0, \tag{14a}$$

$$\phi(t,0) = \phi_0 \sin(\omega_0 t), \quad \phi(t,H) = 0. \tag{14b}$$

Note that we assume blocking electrodes where no electrochemistry occurs, such that the flux of ions through the electrodes is identically zero [Eq. (14a)]. In addition, we neglect the formation of a compact Stern layer at the electrodes. A sinusoidal electric potential of amplitude ϕ_0 and angular frequency $\omega_0 = 2\pi f_0$ is applied on the lower electrode at $z = 0$ while the upper electrode at $z = H$ is kept grounded [Eq. (14b) and Fig. 1]. Here we use the approach outlined by Hashemi Amrei *et al.* [28] to nondimensionlize the system of equations. The electrode spacing H and inverse frequency $1/f_0$ are taken as the characteristic length and timescales, while ϕ_0/H is used to normalize the electric field:

$$\tilde{z} = \frac{z}{H}, \quad \tilde{t} = f_0 t, \quad \tilde{E} = \frac{EH}{\phi_0}. \tag{15}$$

Moreover, for binary 1-1 electrolytes, there are four dimensionless parameters that uniquely describe the system:

$$\Phi_0 = \frac{\phi_0 e}{k_B T}, \quad \delta = \frac{D_-}{D_+}, \quad \kappa H = \sqrt{\frac{n_0 e^2}{\varepsilon k_B T}} H, \quad \mathcal{L}_D = \frac{\sqrt{\hat{D}/f_0}}{H}. \tag{16}$$

Here $n_0 = 2n_\infty$, where n_∞ is the bulk electrolyte concentration, and we have defined $\hat{D} = \sqrt{D_+ D_-}$ as the characteristic diffusivity [28]. Alternatively, we could use the ambipolar diffusivity [32]; however, Hashemi Amrei *et al.* [28] showed that choosing $\hat{D} = \sqrt{D_+ D_-}$ yields accurate predictions of the AREF length scale and its spatial structure, which are key elements of the present study (cf. Sec. III B).

A. Linear solution

A linearized approximate solution to the problem was derived by Hollingsworth and Saville for low applied voltages and equal ionic mobilities (i.e., $\Phi_0 \ll 1$ and $\delta = 1$) [33]. The linearized solution is necessarily unimodal, albeit with phase lag and amplitude that depend on the system properties and location:

$$\tilde{E} = \mathrm{Im}\left[\frac{\alpha \cosh(\alpha\tilde{y}) \operatorname{csch}(\alpha) + i\alpha\nu^2 \coth(\alpha)}{1 + i\alpha\nu^2 \coth(\alpha)} e^{i2\pi\tilde{t}}\right], \tag{17}$$

where $\tilde{y} \equiv 2\tilde{z} - 1$ and the coefficients are

$$\alpha^2 \equiv \frac{1}{4}\left[(\kappa H)^2 + i\frac{2\pi}{\mathcal{L}_D^2}\right], \quad \nu^2 \equiv \frac{2\pi}{(\kappa H)^2 \mathcal{L}_D^2}. \tag{18}$$

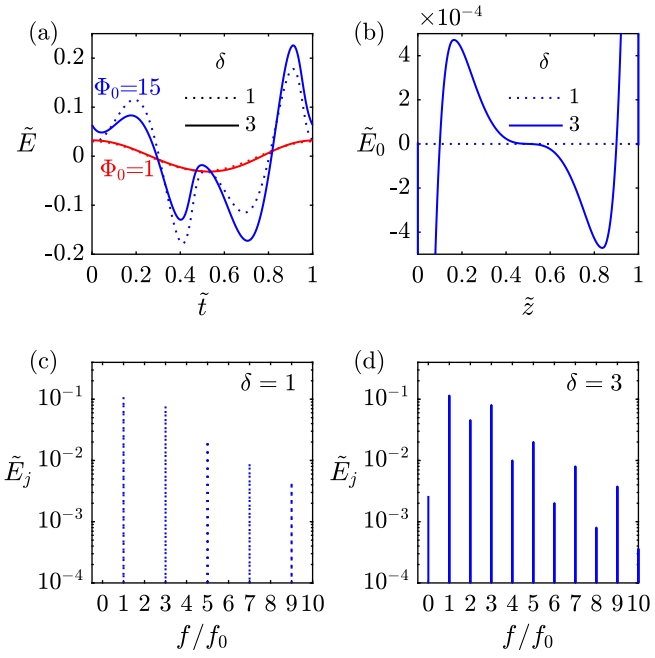

FIG. 2. Representative examples of the one-dimensional AREF. (a) Effect of the applied voltage on time variations of the harmonic electric field ($\tilde{E}$) at $\tilde{z} = 0.04$ for $\delta = 1$ (dashed) and $\delta = 3$ (solid), at applied potentials of $\Phi_0 = 1$ (red) and $\Phi_0 = 15$ (blue). (b) Spatial distribution of the time average electric field ($\tilde{E}_0 = \langle \tilde{E} \rangle$, AREF) for $\delta = 1$ (dashed) and $\delta = 3$ (solid). Note that for $\delta \neq 1$, at locations very close to the electrodes ($\tilde{z} \to 0$ or 1), the AREF reaches a maximum magnitude before sharply decaying toward zero (not discernible here; cf. Refs. [27,28]). (c) and (d) FFT analysis of the harmonic electric field for $\delta = 1$ (c) and $\delta = 3$ (d). Parameters: $\Phi_0 = 15$ (b)–(d), $\mathcal{L}_D = 0.2$, $\kappa H = 2600$.

Note that only two dimensionless groups, κH and $\mathcal{L}_D$, contribute to the approximate linear electric field solution because low applied potential and equal mobilities are assumed. In these limits, then Eq. (17) can be written in the form

$$\tilde{E}(\tilde{t}) = \tilde{E}_1 \cos(2\pi \tilde{t} + \gamma_1), \tag{19}$$

where the amplitude $\tilde{E}_1$ and phase lag γ_1 are functions of both position and the system properties (i.e., κH and $\mathcal{L}_D$). The subscript 1 denotes the frequency mode of the solution; for this unimodal field, there is only one mode corresponding to the applied frequency f_0.

B. Nonlinear solution

As reported by Hashemi Amrei *et al.* [27,28], numerical calculations show that the full nonlinear electrokinetic model yields an electric field with much more complicated spatial and temporal structures than the linearized result. See Refs. [27,28] for details on the numerical methodology and solutions; here we focus on the results and how they pertain to ICEK. Figure 2(a) shows representative examples of the numerically calculated instantaneous electric field versus time at $\tilde{z} = 0.04$ for low and high dimensionless applied voltages and for electrolytes of equal or nonequal ionic mobilities. At the low voltage $\Phi_0 = 1$ and for $\delta = 1$ [Fig. 2(a), dotted red curve, $\Phi_0 = 1$], the electric field solution is a simple unimodal sinusoid consistent with the linearized prediction; indeed, the linearized result in Eq. (17) is not distinguishable from the nonlinear result at this scale. At a higher applied voltages, the contribution from the nonlinear electromigrative terms yield

multimodal peaks [Fig. 2(a), dotted blue curve, $\Phi_0 = 15$]. Qualitatively similar results are obtained for $\delta \neq 1$; the electric field is close to a sinusoid at low voltages and develops nonlinear behavior upon increasing voltage [Fig. 2(a), solid red ($\Phi_0 = 1$) and blue ($\Phi_0 = 15$) curves, respectively].

The time average of the electric field ($E_0 = \langle E \rangle$), however, shows a significant difference between the cases of $\delta = 1$ and $\delta = 3$ [Fig. 2(b)]. For $\delta = 1$ the electric field time average is identically zero everywhere. In contrast, there is a significant nonzero time average electric field (i.e., a DC field) generated for $\delta \neq 1$. The first peak location of this AREF outside the Debye layer closely follows a diffusive length scale, $\tilde{z}_{\text{peak}} \approx 0.83\mathcal{L}_D$ (cf. Fig. 10 of Ref. [28]). Also note that the peak occurs far away from the electrode [≈ 5 μm in Fig. 2(b)]; this behavior, along with the spatially nonuniform AREF, stem from a nonzero time average free charge density far outside the Debye layer. While the magnitude of AREF appears small when compared to the magnitude of the harmonic electric field, the AREF-induced electrophoretic force was shown to be several order of magnitudes larger than gravitational and colloidal forces [27]. Although indiscernible from Fig. 2(b), as $z \to 0$ or 1, within a few Debye lengths from the electrodes, AREF reaches to a peak and then drops toward zero (cf. Refs. [27,28]).

An FFT analysis of the electric field modes shows that for $\delta = 1$ [Fig. 2(c)] the field has frequency components at odd integer multiples of the applied frequency. In other words, the multimodal electric field can be modeled by a sum of sinusoids with frequencies of $f_0, 3f_0, 5f_0, \ldots$ and amplitudes that depend on system properties and location. For $\delta \neq 1$ [Fig. 2(d)], in contrast, the electric field has frequency components at all integer multiples of the applied frequency, including zero (i.e., a steady field). In this case the electric field includes a sum of sinusoids with frequencies of $f_0, 2f_0, 3f_0, \ldots$ plus a steady contribution. Note that the effect of δ on these frequency modes is consistent with a simpler toy model of just two ionic oscillators (see Ref. [27] for details).

Based on these numerical results, the instantaneous nonlinear electric field at any location can be expressed as

$$\tilde{E}(\tilde{t}) = \tilde{E}_0 + \sum_{j=1}^{\infty} \tilde{E}_j \cos(2\pi j\tilde{t} + \gamma_j), \tag{20}$$

where $\tilde{E}_j$ and γ_j are the z-dependent amplitude and phase lag of the frequency component jf_0, respectively. Note that there are two key differences compared to the linearized result [Eq. (19)]. First, the full nonlinear expression has a steady component, $\tilde{E}_0$, whereas the linearized solution does not. Second, the nonlinear expression has an infinite series of all the multiple modes of the imposed frequency, whereas the linear solution is unimodal. In the limit where $\delta \to 1$, the steady component $\tilde{E}_0$ and the even modes $\tilde{E}_{2j} = 0$ for any integer j all vanish. The higher order odd modes, however, are retained even when $\delta \to 1$.

IV. ICEK FLOW WITH AREFs

The sinusoidal nature of the linearized solution [Eq. (19)] indicates that the induced fluid flow pattern is quadrupolar and symmetrical. Substitution of Eq. (19) into Eq. (8) and subsequent time averaging gives the linear ICEK slip velocity as

$$\langle \tilde{u}_\theta^s \rangle = \frac{\langle u_\theta \rangle}{\varepsilon a \phi_0^2/(\mu H^2)} = \tilde{E}_1^2 \frac{\sin(2\theta)}{\omega_0^2 \tau_c^2 + 1}. \tag{21}$$

Inserting the nonlinear electric field solution from Eq. (20) into Eq. (8) and time averaging gives the nonlinear ICEK slip velocity:

$$\langle \tilde{u}_\theta^s \rangle = \sum_{j=1}^{\infty} \left[\tilde{E}_j^2 \frac{\sin(2\theta)}{j^2 \omega_0^2 \tau_c^2 + 1} \right] + 2\tilde{E}_0^2 \sin(2\theta) + 2\tilde{\zeta}_0 \tilde{E}_0 \sin(\theta), \tag{22}$$

where $\tilde{\zeta}_0 = \frac{\zeta_0 H}{a\phi_0}$. Note that Eq. (22) has three contributions: (1) an ICEK quadrupolar flow due to the first and all higher order modes of the nonlinear field, (2) an ICEK quadrupolar flow due to the steady AREF, and (3) an electroosmotic dipolar flow due to the action of the steady AREF on the intrinsic charge on the cylinder. For $\delta = 1$ ($\tilde{E}_0 = 0$), as voltage goes to zero $\tilde{E}_{j\neq 1} \to 0$, and the nonlinear and linear slip velocities asymptotically converge. Unlike the linear slip velocity which predicts an invariably quadrupolar and symmetrical fluid flow, the nonlinear one is in general asymmetrical due to the dipolar electroosmotic term stemming from the steady field component. In other words, any mismatch in the mobilities of the dissolved ions breaks the symmetry and induces net fluid flow around a charged cylinder under AC polarization.

As discussed in detail by Hashemi Amrei *et al.* [28], $\tilde{E}_0$ and $\tilde{E}_j$ are complicated functions of the four dimensionless parameters Φ_0, $\mathcal{L}_D$, δ, and κH. Equation (22) introduces two more dimensionless groups, $\tilde{\zeta}_0$ and $\omega_0\tau_c$, that also affect the flow behavior. Under typical experimental conditions, however, $\omega_0\tau_c \ll 1$ and its impact is negligible; we do not consider it further here. A parameter that is important, however, is the location of the cylinder between the two electrodes (i.e., h), which is included in the dimensionless group $\tilde{h} = h/H$. In other words, the flow structure and magnitude is governed by the six dimensionless parameters Φ_0, $\mathcal{L}_D$, δ, κH, $\tilde{\zeta}_0$, and $\tilde{h}$.

Using the slip velocity given by Eq. (22) for nonlinear ICEK, we find the radial velocity, angular velocity, and corresponding stream function around the charged cylinder are, respectively,

$$\tilde{u}_r = \left(\frac{1}{\tilde{r}^2} - 1\right)\tilde{\zeta}_0\tilde{E}_0\cos(\theta) + 2\left(\frac{1-\tilde{r}^2}{\tilde{r}^3}\right)\tilde{E}_0^2 + \sum_{j=1}^{\infty}\left(\frac{1-\tilde{r}^2}{\tilde{r}^3}\right)\frac{\tilde{E}_j^2}{\left(\omega_0^2\tau_c^2+1\right)}\cos(2\theta), \tag{23a}$$

$$\tilde{u}_\theta = \left(\frac{1}{\tilde{r}^2} + 1\right)\tilde{\zeta}_0\tilde{E}_0\sin(\theta) + \frac{2}{\tilde{r}^3}\tilde{E}_0^2\sin(2\theta) + \sum_{j=1}^{\infty}\frac{1}{\tilde{r}^3}\frac{\tilde{E}_j^2}{\left(\omega_0^2\tau_c^2+1\right)}\sin(2\theta), \tag{23b}$$

$$\tilde{\Psi} = \left(\frac{1}{\tilde{r}} - \tilde{r}\right)a\tilde{\zeta}_0\tilde{E}_0\sin(\theta) + \left(\frac{1}{\tilde{r}^2} - 1\right)a\tilde{E}_0^2\sin(2\theta) + \sum_{j=1}^{\infty}\left(\frac{1}{\tilde{r}^2} - 1\right)\frac{a\tilde{E}_j^2}{2\left(\omega_0^2\tau_c^2+1\right)}\sin(2\theta). \tag{23c}$$

Here $\tilde{\Psi} = \Psi\mu H^2/(\varepsilon a^2\phi_0^2)$ is the dimensionless stream function and $\tilde{r} = r/a$. (Please refer to the Appendix for detailed derivation.) For linear ICEK, note that the velocity and stream function are simply expressed by the first series terms on the right-hand side of Eq. (23) (i.e., $\tilde{E}_j = 0$ for $j \neq 1$).

The streamlines for the linearized solution are invariably quadrupolar, i.e., the shape of the flow never changes in the linearized field limit (although the flow velocity varies). In contrast, the flow structure for the full nonlinear solution is highly sensitive to the system parameters. Representative streamlines for the induced fluid flows from the nonlinear solution are provided in Fig. 3. Focusing first on the mobility mismatch [Fig. 3(a)], the fluid flow pattern for an electrolyte with $\delta = 1$ is perfectly quadrupolar. In contrast, electrolytes with an ionic mobility mismatch ($\delta \neq 1$) generate a net fluid flow as a result of the dipolar contribution of the slip velocity (i.e., standard electroosmosis due to the AREF). Note that the direction of the fluid flow depends sensitively on the magnitude of δ; in other words, swapping out an electrolyte with $\delta < 1$ (e.g., HCl) with an electrolyte that has $\delta > 1$ (e.g., NaOH) and holding all other parameters constant will result in a reversal in the direction of flow.

A similar flow reversal also occurs for different magnitudes of the frequency-dependent diffusive length scale, $\mathcal{L}_D$ [Fig. 3(b)]. For sufficiently large values of $\mathcal{L}_D$, i.e., sufficiently low frequencies, the fluid flow is dominated by the dipolar steady AREF-driven electroosmosis. For $\mathcal{L}_D = 0.55$ and $\tilde{h} = 0.2$ the flow is directed downward (in the negative z direction). This particular directionality stems from the direction of the steady field component at this specific frequency and location. As discussed by Hashemi Amrei *et al.* [28], the direction of the steady field at a given location depends sensitively on the applied frequency; note in Fig. 2(b) that the direction of the field is negative for $0 < \tilde{z} < 0.1$, positive for $0.1 < \tilde{z} < 0.5$, and antisymmetric for $\tilde{z} > 0.5$. The precise positions

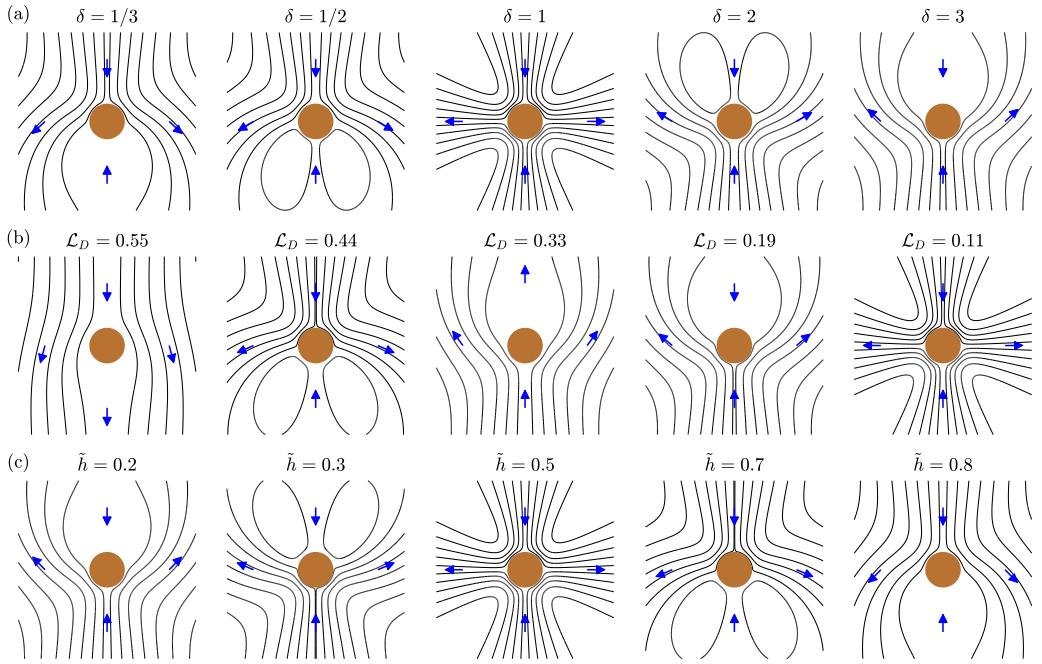

FIG. 3. Effects of (a) mobility mismatch, (b) frequency-dependent diffusive length scale, and (c) cylinder position on the induced fluid flow pattern around the cylinder, as calculated using Eq. (21) and the nonlinear solution to the standard electrokinetic model [cf. Eq. (19)]. Parameters: $\Phi_0 = 10$, $\delta = 3$ (b), (c), $\mathcal{L}_D = 0.2$ (a), (c), $\kappa H = 2600$, $\tilde{\zeta}_0 = -10$, $\tilde{h} = 0.22$ (a), (b).

where the field direction changes depend on frequency, with more zeros in the field strength (i.e., reversals in the field direction) as frequency increases ($\mathcal{L}_D$ decreases). The corresponding flow thus changes dramatically, with the direction of the steady dipolar flow switching as $\mathcal{L}_D$ decreases to 0.33 [Fig. 3(b)]. Further decreases in $\mathcal{L}_D$ (increases in frequency) further diminish the dipolar contribution, and the fluid flow pattern becomes increasingly quadrupolar because $\tilde{E}_0$ at this particular location tends to decrease as $\mathcal{L}_D$ decreases. The effect of cylinder location, with all other parameters fixed, is shown in Fig. 3(c). At the midplane (i.e., $\tilde{h} = 0.5$) where AREF necessarily vanishes due to symmetry, the fluid flow is entirely quadrupolar. Away from the midplane (any location $\tilde{h} \neq 0.5$), there can be a net dipolar flow induced with direction dependent on the sign of AREF.

We emphasize that the exact conditions upon which the flow reversal occurs is a sensitive function of all six dimensionless parameters governing the system behavior and the location of the cylinder, due to the complicated spatial structure of AREF [28]. Linearized theories with slip velocity given by Eq. (21) will not capture these flow reversals, which are a direct result of ionic mobility mismatch and the consquent AREF. In other words, solutions to the full nonlinear problem with $\delta \neq 1$ will yield flow reversals, whereas more sophisticated solutions to the electrokinetic model at high voltages [26,34,35], but with the assumption of equal ionic mobilities, will not.

To further quantify the induced flow behavior, the effects of the dimensionless parameters on the scalar component of the fluid velocity in θ direction ($\tilde{u}_\theta$) at a fixed location of $r = 2a$ and $\theta = \pi/6$ are shown in Fig. 4. We stress that these results are not general; the curves and critical values of flow reversal are crucially dependent on the system properties and complicated spatial structure of the AREF. Figure 4(a) shows the effect of mobility mismatch (δ) on $\tilde{u}_\theta$ at three different applied potentials. Changes in δ have no impact on the linear solution, but δ dramatically affects the predictions of the nonlinear solution. As expected, at a low voltage of $\Phi_0 = 1$, the linear and nonlinear solutions

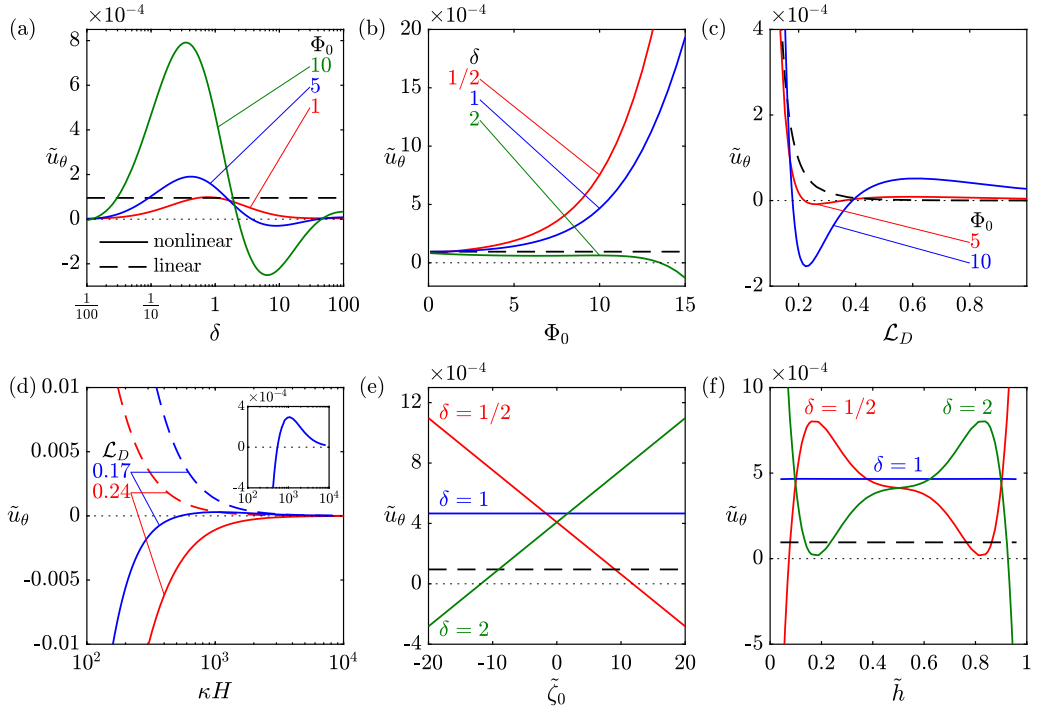

FIG. 4. Influence of the six dimensionless parameters that govern $\tilde{u}_\theta^s$, evaluated at $r = 2a$ and $\theta = \pi/6$. In all figures, dashed black lines represent the velocity calculated using the linearized electric field, while solid colored lines represent the velocity calculated using the full nonlinear solution for various parametric values. Parameters: $\Phi_0 = 10$ (d)–(f), $\delta = 3$ (c), (d), $\mathcal{L}_D = 0.2$ (a), (b), (e), (f), $\kappa H = 2600$ (a)–(c), (e), (f), $\tilde{\zeta}_0 = -10$ (a)–(d), (f), $\tilde{h} = 0.22$ (a)–(e). The inset of (d) shows a magnification of the nonlinear solution for $\mathcal{L}_D = 0.17$.

converge at $\delta = 1$. At higher voltages, however, even when the steady AREF component is zero for $\delta = 1$, there is a considerable difference between the linear and nonlinear predicted velocities, stemming from the contribution of the higher order frequency modes. Furthermore, changing the mobility mismatch alters the fluid flow both qualitatively and quantitatively. For instance, at $\Phi_0 = 10$, the fluid velocity varies from $\tilde{u}_\theta \approx 4.5\times10^{-4}$ at $\delta = 1.04$ (e.g., KCl) to $\approx -2\times10^{-4}$ at δ=3.95 (e.g., NaOH).

An important point to consider, as discussed in Ref. [28], is that the effect of δ is nonmonotonic. The AREF is always identically zero at $\delta = 1$, and vanishes as $\delta \to \infty$. Where the peak AREF magnitude occurs as a function of δ, however, depends on the applied voltage. At low voltages, the peak occurs near $\delta \approx 5$ (or $\delta \approx 1/5$). Thus in the representative examples shown in Fig. 4(a), the absolute magnitude of the velocity tends to peak near $\delta \approx 5$ and $\delta \approx 1/5$; for the range of Φ_0 shown here, these are the specific values of δ where the field strength is greatest. As the applied voltage increases, however, the AREF peaks in magnitude at values of δ closer to 1. In other words, at higher voltages, AREF in electrolytes with δ close to 1 (e.g., KCl with $\delta \approx 1.04$) might be stronger than that in electrolytes with a significant ionic mobility mismatch (e.g., NaOH with $\delta \approx 3.95$). Indeed, many of the peculiar experimental observations such as fluid flow reversal upon changing the frequency and voltage were reported for KCl electrolyte at relatively large voltages [7,10,20,36].

The effect of the applied potential Φ_0 is shown in Fig. 4(b) for different values of δ. Again, the linearized dimensionless solution is insensitive to changes in Φ_0; dimensionally, the flow is predicted to increase as ϕ_0^2 [cf. Eq. (21)]. At low applied voltages and regardless of δ, the nonlinear

solution approaches the linear solution (dashed black curve). As Φ_0 increases, however, the velocity increases rapidly, i.e., the velocity increases faster than quadratically. For $\delta = 1/2$, the increase is even steeper. Interestingly, for $\delta = 2$, increasing the applied voltage sufficiently will alter the fluid flow direction. In contrast, for cases of $\delta = 1$ and $\delta = 1/2$ it is only the magnitude of $\tilde{u}_\theta$ that is affected by Φ_0 and no change in direction is observed.

Figure 4(c) illustrates the effect of $\mathcal{L}_D$ on the fluid velocity. The linear solution predicts an exponential decay in $\tilde{u}_\theta$ with no direction change. In contrast, the nonlinear solution predicts multiple direction changes upon varying $\mathcal{L}_D$. Recalling that the dimensionless parameter $\mathcal{L}_D$ has an inverse frequency dependence [Eq. (16)], increasing $\mathcal{L}_D$ can be seen as deceasing the applied frequency f_0. Therefore, the results indicate how solutions to the full nonlinear electrokinetic model are capable of capturing the fluid flow reversal by changing the applied frequency.

The effect of κH on the induced fluid velocity is depicted in Fig. 4(d) for two different values of $\mathcal{L}_D$. The results are presented only for high κH values, where the assumption of $\omega_0 \tau_c \ll 1$ holds. Note that for the most part the linear and nonlinear solutions predict the fluid flow in opposite directions, which is a consequence of $\delta \neq 1$ [cf. Fig. 4(a)]. The magnitudes of both the linear and nonlinear solutions drop by increasing κH, which corresponds to increasing the ionic concentration. At higher concentrations, the Debye layer shrinks and it becomes less effective in micron scale electrokinetic phenomena. Likewise, some experimental studies have reported a strong concentration dependence of the fluid velocity magnitude in ACEO micropumps that tends to strongly suppress the flows [7,20]. Hence, any future interpretation of the concentration effect in ACEO pumps and similar systems should take into account the potentially confounding impact of AREFs. Also, a peculiar direction change in the nonlinear solution happens for the case of $\mathcal{L}_D = 0.17$ at $\kappa H \approx 500$. This result is qualitatively similar to a flow reversal with electrolyte concentration that was reported in a different geometry of ACEO experiments [20].

Figure 4(e) demonstrates the effect of dimensionless zeta potential $\tilde{\zeta}_0$ on the fluid velocity. The linear solution prediction has no electroosmotic contribution, making it insensitive to $\tilde{\zeta}_0$. Regarding the nonlinear solution, for $\delta = 1$, AREF is zero and again the cylinder charge has no impact on the fluid velocity. When $\delta \neq 1$ however, the fluid velocity linearly depends on the zeta potential, but with direction that depends on the sign of the AREF.

Finally, the location of the cylinder $\tilde{h}$ has a significant impact on the fluid velocity distribution. As shown in Fig. 4(f), the linear solution has no dependency on $\tilde{h}$, at least when, like in all practical examples, the cylinder is placed far outside the Debye layer ($\kappa H \tilde{h} \gg 1$ and $\kappa H(1 - \tilde{h}) \gg 1$ for $\tilde{h} < 1/2$ and $\tilde{h} > 1/2$, respectively). For the nonlinear solution and for $\delta = 1$, again the cylinder location does not affect the model predictions. This location independence is due to the fact that AREF, which is responsible for the spatial nonuniformity of the electric field, is zero when $\delta = 1$. Therefore, we conclude that for electrolytes with $\delta = 1$, regardless of the cylinder location, the fluid flow pattern would be quadrupolar. When $\delta \neq 1$, interesting behavior is observed [Fig. 4(f), $\delta = 1/2$ and 2]. Changing the location dramatically alters both the magnitude and direction of the fluid velocity. Moreover, the cases of $\delta = 1/2$ and 2 predict the same fluid velocity at the midplane. Knowing that AREF is always zero at the midplane, the fluid flow pattern would again be quadrupolar there, regardless of the precise value of δ.

V. CONCLUSIONS

A key implication of the results presented here is that they point toward a resolution of long-standing shortfalls of the ICEK theory, in particular the reversals in fluid flow direction upon changes in the applied frequency and electrolyte type in AC electroosmosis pumps. To our knowledge, the model presented here is the first to predict a flow reversal in an ICEK system that retains the continuum approximation, i.e., without invoking finite ion size or crowding effects. The model predicts that the flow structure will depend sensitively on several dimensionless parameters, including ionic mobility mismatch ($\delta = D_-/D_+$), diffusive length scale ($\mathcal{L}_D$, defined based on the applied frequency), and even the location of cylinder between the electrodes, all of which complicate

experimental interpretation. To date, all reported experiments on ICEK around charged cylinders or spheres have placed the object exactly at the midplane between the two electrodes, or used an electrolyte solution with $\delta \approx 1$ (e.g., KCl). In both of these cases, the results provided here predict a quadrupolar fluid flow pattern, in qualitative agreement to the experiments. We are unaware of published experimental results where the object is placed at a location other than the midplane in an electrolyte with $\delta \neq 1$.

A key limitation of our model is that it pertains only in the limits $a/h \ll 1$ and $a/H \ll 1$, so that the presence of the cylinder has negligible impact on the electric field distribution obtained from the one-dimensional solution. An improved model would take into account the effect of the cylinder presence on the electric field itself, and how that alters the consequent flow. Such a full two-dimensional numerical simulation for the electrokinetic equations will remove the necessity of the above assumptions and will provide a better understanding of the phenomena. Likewise, ACEO pumps intrinsically involve two-dimensional electrode arrays, so the influence of AREFs in these systems will also require more sophisticated numerical techniques. Furthermore, we focused here on the consequence of asymmetries in the ionic mobility and cylinder position, but the symmetry of the system can be broken in other ways, including in the shape and/or surface chemistry of the object or the applied electric field gradient, all of which have been shown to generate net fluid flows and electrophoretic motion of conducting particles [8,37–39]. Finally, we focused here on dilute solutions, but transport in more concentrated solutions will require consideration of Stefan-Maxwell coupled ionic fluxes [32,40]. The influence of AREFs on ICEK flows in two-dimensional systems with these more complicated broken symmetries is deferred to future studies.

ACKNOWLEDGMENT

This material is based upon work partially supported by the National Science Foundation under Grant No. DMS-1664679.

APPENDIX: VELOCITY PROFILES AND STREAMLINES

Given the time average slip velocity in θ direction around the surface of a cylinder ($\langle u_\theta^s \rangle$), the time average fluid flow profile [$u_r(r,\theta)$ and $u_\theta(r,\theta)$] is derived. We consider two different cases of standard electroosmosis (EOS) and induced-charge electrokinetics (ICEK).

1. Standard electroosmosis (EOS)

For a cylinder of radius a and intrinsic surface zeta potential of ζ_0 subject to a far-field $E(t) = E$, the slip velocity due to standard electroosmosis is given by

$$\left\langle u_\theta^s \right\rangle = -\frac{\varepsilon \zeta_0 E_\theta|_{r=a}}{\mu} = 2\frac{\varepsilon \zeta_0 E}{\mu} \sin(\theta) = 2U \sin(\theta). \tag{A1}$$

We use stream function to solve this axisymmetric flow problem [41]. For a steady, creeping flow, the stream function equation is

$$\left[\frac{1}{r}\frac{\partial}{\partial r}\left(r\frac{\partial}{\partial r}\right) + \frac{1}{r^2}\frac{\partial^2}{\partial \theta^2}\right]^2 \Psi = 0, \quad u_r = \frac{1}{r}\frac{\partial \Psi}{\partial \theta}, \quad u_\theta = -\frac{\partial \Psi}{\partial r}, \tag{A2}$$

subject to the following boundary conditions at $r = a$:

$$u_r(a,\theta) = 0, \quad u_\theta(a,\theta) = \langle u_\theta^s \rangle. \tag{A3}$$

In addition, as $r \to \infty$ the velocities must remain finite.

We now guess a solution of the form

$$\Psi = f(r) \sin\theta. \tag{A4}$$

On substitution into Eq. (A2) we get

$$r^4 f'''' + 2r^3 f''' - 3r^2 f'' + 3rf' - 3f = 0. \tag{A5}$$

Inserting $f = cr^n$, we find the roots as $n = -1, 3$ and a double root for $n = 1$. The latter yields $r\ln(r)$ as another linearly independent solution. Therefore, the general solution to the stream function equation [Eq. (A2)] becomes

$$\Psi = \left[\frac{c_1}{r} + c_2 r + c_3 r\ln(r) + c_4 r^3\right]\sin(\theta), \tag{A6}$$

which subsequently yields the velocity distributions as

$$u_r = \left[\frac{c_1}{r^2} + c_2 + c_3\ln(r) + c_4 r^2\right]\cos(\theta), \quad u_\theta = \left\{\frac{c_1}{r^2} - c_2 - c_3[\ln(r) + 1] - 3c_4 r^2\right\}\sin(\theta). \tag{A7}$$

For velocities to remain finite far from the cylinder, c_3 and c_4 must be zero. Finally, applying the boundary conditions at $r = a$ from Eq. (A3), we find the velocity distributions and stream function as

$$u_r = \left(\frac{1}{\tilde{r}^2} - 1\right)U\cos(\theta), \tag{A8a}$$

$$u_\theta = \left(\frac{1}{\tilde{r}^2} + 1\right)U\sin(\theta), \tag{A8b}$$

$$\Psi = \left(\frac{1}{\tilde{r}} - \tilde{r}\right)aU\sin(\theta), \tag{A8c}$$

where $\tilde{r} = r/a$.

2. Induced-charge electrokinetics (ICEK)

The slip velocity for ICEK is given by

$$\langle u_\theta^s\rangle = 2\frac{\varepsilon a E^2}{\mu}\sin 2\theta, \tag{A9}$$

for a steady field $E(t) = E$, and

$$\langle u_\theta^s\rangle = \frac{\varepsilon a E^2}{\mu\left(\omega_0^2\tau_c^2 + 1\right)}\sin 2\theta, \tag{A10}$$

for an oscillatory electric field $E(t) = E\cos(\omega_0 t + \gamma)$. For generality, we write

$$\langle u_\theta^s\rangle = 2U\sin 2\theta, \tag{A11}$$

where the U expression depends on the electric field type.

This time we guess $\Psi = f(r)\sin(2\theta)$ and insert into Eq. (A2) to get

$$r^4 f'''' + 2r^3 f''' - 9r^2 f'' + 9rf' = 0. \tag{A12}$$

Substituting $f = cr^n$, the roots are obtained as $n = -2, 0, 2, 4$; therefore the general solution is

$$\Psi = \left(\frac{c_1}{r^2} + c_2 + c_3 r^2 + c_4 r^4\right)\sin(2\theta). \tag{A13}$$

The scalar velocity components are therefore

$$u_r = 2\left(\frac{c_1}{r^3} + \frac{c_2}{r} + c_3 r + c_4 r^3\right)\cos(2\theta), \quad u_\theta = \left(\frac{2c_1}{r^3} - 2c_3 r - 4c_4 r^3\right)\sin(2\theta). \tag{A14}$$

Again, the condition of finite velocities as $r \to \infty$, eliminates c_3 and c_4 terms. Applying the boundary conditions at $r = a$ [Eq. (A3)], the final forms of the velocity and stream function profiles are obtained as

$$u_r = 2\left(\frac{1-\tilde{r}^2}{\tilde{r}^3}\right)U\cos(2\theta), \tag{A15a}$$

$$u_\theta = \frac{2}{\tilde{r}^3}U\sin(2\theta), \tag{A15b}$$

$$\Psi = \left(\frac{1}{\tilde{r}^2}-1\right)aU\sin(2\theta). \tag{A15c}$$

3. Superposition

Now consider an electric field of the form

$$E(t) = E_0 + \sum_{j=1}^{\infty} E_j \cos(j\omega_0 t + \gamma_j). \tag{A16}$$

By superposition one can find the distributions of scalar velocity components and stream function as given in Eq. (23).

[1] N. I. Gamayunov, V. A. Murtsovkin, and A. S. Dukhin, Pair interaction of particles in electric-field. 1. Features of hydrodynamic interaction of polarized particles, Colloid J. **48**, 197 (1986).

[2] A. S. Dukhin and V. A. Murtsovkin, Pair interaction of particles in electric-field. 2. Influence of polarization of double-layer of dielectric particles on their hydrodynamic interaction in a stationary electric-field, Colloid J. **48**, 203 (1986).

[3] A. S. Dukhin, Pair interaction of disperse particles in electric-field. 3. Hydrodynamic interaction of ideally polarizable metal particles and dead biological cells, Colloid J. **48**, 376 (1986).

[4] A. Ramos, H. Morgan, N. G. Green, and A. Castellanos, Ac electrokinetics: A review of forces in microelectrode structures, J. Phys. D **31**, 2338 (1998).

[5] A. Ramos, H. Morgan, N. G. Green, and A. Castellanos, Ac electric-field-induced fluid flow in microelectrodes, J. Colloid Interface Sci. **217**, 420 (1999).

[6] A. Ajdari, Pumping liquids using asymmetric electrode arrays, Phys. Rev. E **61**, R45(R) (2000).

[7] V. Studer, A. Pepin, Y. Chen, and A. Ajdari, An integrated ac electrokinetic pump in a microfluidic loop for fast and tunable flow control, Analyst **129**, 944 (2004).

[8] M. Z. Bazant and T. M. Squires, Induced-Charge Electrokinetic Phenomena: Theory and Microfluidic Applications, Phys. Rev. Lett. **92**, 066101 (2004).

[9] T. M. Squires and M. Z. Bazant, Induced-charge electro-osmosis, J. Fluid Mech. **509**, 217 (2004).

[10] M. Z. Bazant, M. S. Kilic, B. D. Storey, and A. Ajdari, Towards an understanding of induced-charge electrokinetics at large applied voltages in concentrated solutions, Adv. Colloid Interface Sci. **152**, 48 (2009).

[11] T. M. Squires, Induced-charge electrokinetics: Fundamental challenges and opportunities, Lab Chip **9**, 2477 (2009).

[12] M. Z. Bazant and T. M. Squires, Induced-charge electrokinetic phenomena, Curr. Opin. Colloid Interface Sci. **15**, 203 (2010).

[13] A. Ramos, P. Garcia-Sanchez, and H. Morgan, Ac electrokinetics of conducting microparticles: A review, Curr. Opin. Colloid Interface Sci. **24**, 79 (2016).

[14] N. I. Gamayunov, G. I. Mantrov, and V. A. Murtsovkin, Study of flows induced in the vicinity of conducting particles by an external electric-field, Colloid J. **54**, 20 (1992).

[15] C. Peng, I. Lazo, S. V. Shiyanovskii, and O. D. Lavrentovich, Induced-charge electro-osmosis around metal and Janus spheres in water: Patterns of flow and breaking symmetries, Phys. Rev. E **90**, 051002 (2014).
[16] J. A. Levitan, S. Devasenathipathy, V. Studer, Y. Ben, T. Thorsen, T. M. Squires, and M. Z. Bazant, Experimental observation of induced-charge electro-osmosis around a metal wire in a microchannel, Colloids Surf. A **267**, 122 (2005).
[17] C. Canpolat, S. Qian, and A. Beskok, Micro-piv measurements of induced-charge electro-osmosis around a metal rod, Microfluid Nanofluid **14**, 153 (2013).
[18] H. Feng, Y. Huang, T. N. Wong, and F. Duan, Electrolyte effect in induced charge electroosmosis, Soft Matter **13**, 4864 (2017).
[19] J. P. Urbanski, T. Thorsen, J. A. Levitan, and M. Z. Bazant, Fast ac electro-osmotic micropumps with nonplanar electrodes, Appl. Phys. Lett. **89**, 143508 (2006).
[20] M. Z. Bazant, J. P. Urbanski, J. A. Levitan, K. Subramanian, M. S. Kilic, A. Jones, and T. Thorsen, Electrolyte dependence of ac electro-osmosis, in *Micro Total Analysis Systems 2007* (Chemical and Biological Microsystems Society, 2007), Vol. 1.
[21] B. D. Storey, L. R. Edwards, M. S. Kilic, and M. Z. Bazant, Steric effects on ac electro-osmosis in dilute electrolytes, Phys. Rev. E **77**, 036317 (2008).
[22] P. Garcia-Sanchez, A. Ramos, A. Gonzalez, N. G. Green, and H. Morgan, Flow reversal in traveling-wave electrokinetics: An analysis of forces due to ionic concentration gradients, Langmuir **25**, 4988 (2009).
[23] M. S. Kilic, M. Z. Bazant, and A. Ajdari, Steric effects in the dynamics of electrolytes at large applied voltages. I. Double-layer charging, Phys. Rev. E **75**, 021502 (2007).
[24] M. S. Kilic, M. Z. Bazant, and A. Ajdari, Steric effects in the dynamics of electrolytes at large applied voltages. II. modified Poisson-Nernst-Planck equations, Phys. Rev. E **75**, 021503 (2007).
[25] M. Z. Bazant, M. S. Kilic, B. D. Storey, and A. Ajdari, Nonlinear electrokinetics at large voltages, New J. Phys. **11**, 075016 (2009).
[26] L. Højgaard Olesen, M. Z. Bazant, and H. Bruus, Strongly nonlinear dynamics of electrolytes in large ac voltages, Phys. Rev. E **82**, 011501 (2010).
[27] S. M. H. Hashemi Amrei, S. C. Bukosky, S. P. Rader, W. D. Ristenpart, and G. H. Miller, Oscillating Electric Fields in Liquids Create a Long-Range Steady Field, Phys. Rev. Lett. **121**, 185504 (2018).
[28] S. M. H. Hashemi Amrei, G. H. Miller, and W. D. Ristenpart, Asymmetric rectified electric fields between parallel electrodes: Numerical and scaling analyses, Phys. Rev. E **99**, 062603 (2019).
[29] S. C. Bukosky, S. M. H. Hashemi Amrei, S. P. Rader, J. Mora, G. H. Miller, and W. D. Ristenpart, Extreme levitation of colloidal particles in response to oscillatory electric fields, Langmuir **35**, 6971 (2019).
[30] M. Z. Bazant, K. Thornton, and A. Ajdari, Diffuse-charge dynamics in electrochemical systems, Phys. Rev. E **70**, 021506 (2004).
[31] W. B. Russel, D. A. Saville, and W. R. Schowalter, *Colloidal Dispersions* (Cambridge University Press, Cambridge, 1991).
[32] B. Balu and A. S. Khair, Role of stefan-maxwell fluxes in the dynamics of concentrated electrolytes, Soft Matter **14**, 8267 (2018).
[33] A. D. Hollingsworth and D. A. Saville, A broad frequency range dielectric spectrometer for colloidal suspensions: Cell design, calibration, and validation, J. Colloid Interface Sci. **257**, 65 (2003).
[34] O. Schnitzer and E. Yariv, Nonlinear oscillations in an electrolyte solution under ac voltage, Phys. Rev. E **89**, 032302 (2014).
[35] R. F. Stout and A. S. Khair, Moderately nonlinear diffuse-charge dynamics under an ac voltage, Phys. Rev. E **92**, 032305 (2015).
[36] P. Garcia-Sanchez, A. Ramos, N. G. Green, and H. Morgan, Experiments on ac electrokinetic pumping of liquids using arrays of microelectrodes, IEEE Trans. Dielectr. Electr. Insul. **13**, 670 (2006).
[37] T. M. Squires and M. Z. Bazant, Breaking symmetries in induced-charge electro-osmosis and electrophoresis, J. Fluid Mech. **560**, 65 (2006).
[38] S. Gangwal, O. J. Cayre, M. Z. Bazant, and O. D. Velev, Induced-Charge Electrophoresis of Metallodielectric Particles, Phys. Rev. Lett. **100**, 058302 (2008).

[39] A. Boymelgreen, G. Yossifon, S. Park, and T. Miloh, Spinning Janus doublets driven in uniform ac electric fields, Phys. Rev. E **89**, 011003 (2014).

[40] S. T. P. Psaltis and T. W. Farrell, Comparing charge transport predictions for a ternary electrolyte using the Maxwell-Stefan and Nernst-Planck equations, J. Electrochem. Soc. **158**, A33 (2011).

[41] R. B. Bird, W. E. Stewart, and E. N. Lightfoot, *Transport Phenomena*, 2nd ed. (John Wiley & Sons, New York, 2002).